Measuring E and B Fields in Laser-Produced Plasmas with Monoenergetic Proton Radiography

C. K. Li, F. H. Séguin, J. A. Frenje, J. R. Rygg, and R. D. Petrasso
Plasma Science and Fusion Center, Massachusetts Institute of Technology, Cambridge, Massachusetts 02139, USA

R. P. J. Town, P. A. Amendt, S. P. Hatchett, O. L. Landen, A. J. Mackinnon, and P. K. Patel
Lawrence Livermore National Laboratory, Livermore, California 94550, USA

V. A. Smalyuk, T. C. Sangster, and J. P. Knauer
Laboratory for Laser Energetics, University of Rochester, Rochester, New York 14623, USA
(Received 2 June 2006; published 28 September 2006)

Electromagnetic (E/B) fields generated by the interaction with plasmas of long-pulse, low-intensity laser beams relevant to inertial confinement fusion have been measured for the first time using novel monoenergetic proton radiography methods. High-resolution, time-gated radiography images of a plastic foil driven by a 10^{14} W/cm^2 laser implied B fields of $\sim$0.5 MG and E fields of $\sim 1.5 \times 10^8$ V/m. Simulations of these experiments with LASNEX + LSP have been performed and are in overall (though not exact) agreement with the data both for field strengths and for spatial distributions; this is the first direct experimental test of the laser-generated B-field package in LASNEX. The experiments also demonstrated that laser phase plates substantially reduce medium-scale chaotic field structure.

DOI: 10.1103/PhysRevLett.97.135003 PACS numbers: 52.38.Fz, 52.50.Jm, 52.70.Nc

The generation of electromagnetic fields (E/B) by interactions of laser light with matter is a process of fundamental interest in high-energy-density (HED) physics [1]. The primary mechanism behind field formation is the loss of energetic electrons from the heated region, resulting in the breakdown of neutrality. Many processes can then contribute to field generation and evolution, but their relative importance depends on interaction parameters [1–5]. For long-pulse, low-intensity laser light, the dominant source for B field generation is noncollinear electron density and temperature gradients ($\nabla n_e \times \nabla T_e$); the dominant source for E fields is $\nabla P/n_e$ [1–5]. For circular laser spots, the B fields have a toroidal configuration with scale length comparable to the spot size. In the regime with low Z and high T_e, where resistivity is low, B-field growth is usually linear in time and is balanced primarily by convective losses (i.e., the B field is "frozen in"). Under these circumstances, B field evolution can be described by the Faraday equation combined with a simplified version of the generalized Ohm's law,

$$\frac{\partial \mathbf{B}}{\partial t} \approx \nabla \times (\mathbf{v} \times \mathbf{B}) - \frac{1}{e n_e} \nabla n_e \times \nabla T_e, \qquad (1)$$

where $\mathbf{v}$ is the plasma fluid velocity.

In addition to its importance to fundamental HED physics, these fields have important implications for several current problems. In inertial confinement fusion (ICF), B fields ($\sim$ MG) are generated inside a hohlraum by long-pulse ($\sim$ 1 ns) laser illumination [6–8]. Such fields can reduce heat flow, since cross-field thermal conductivity is modified by a factor of $(1 + \omega_{ce}{}^2 \tau^2)^{-1}$, where ω_{ce} is the electron gyrofrequency and τ is the collision time. The result is altered distributions of T_e and n_e, enhancing laser-plasma instabilities and implosion asymmetries [6–8]. The experiments described here are the first to directly measure fields generated by the types of laser beams used in direct- and indirect-drive ICF.

Previous work focused on short-pulse, high-intensity lasers [9–11], and field measurements were based on Faraday rotation [10], probes [4], or high-order laser harmonics [11]. It has also been proposed that proton radiography could provide a method for measuring fields through the deflections they induce in proton trajectories; Mackinnon *et al.* [12] demonstrated that high-resolution images containing deflection information could be obtained, although no direct connections were made between images and fields, while Romagnani *et al.* [13] utilized side-on proton radiography to study E fields. In both experiments, fields and probing protons were generated by short-pulse, high-intensity lasers, and the backlighting sources had a large proton flux with continuous energy spectrum.

We recently developed a novel imaging technology combining a monoenergetic proton backlighter with a matched detection system [14,15]. Protons are generated as fusion products from the reaction $D + {}^3\mathrm{He} \rightarrow \alpha + p$ in exploding-pusher implosions of D^3He-filled, glass-shell capsules [16]; the proton birth energy is $E_p = 14.7$ MeV, with a small amount of thermal broadening. For the experiments described here, backlighter implosions were driven by 20 OMEGA laser beams; a typical measured proton spectrum is shown in Fig. 1, indicating a proton yield of $\sim 3 \times 10^8$. The spatial size of the proton source was measured with a proton-emission imaging system [17], which determined that the source was nearly spherical and had approximately a Gaussian radial emission profile with

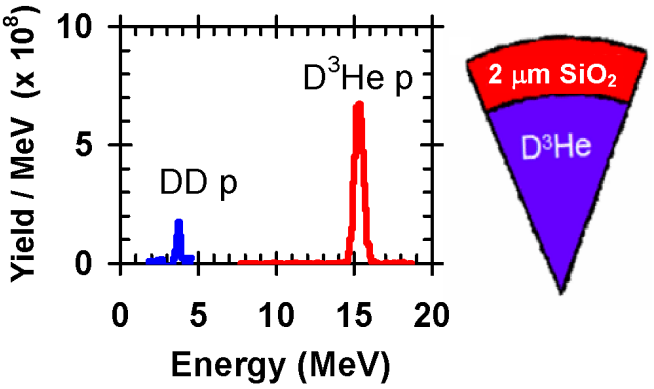

FIG. 1 (color online). Measured energy spectra of monoenergetic D^3He and DD protons generated in an implosion of a thin-glass shell filled with D^3He gas (OMEGA shot 42767). The data described in this Letter correspond to the D^3He protons.

FWHM ~45 μm. Timing of proton production was measured by a proton temporal diagnostic (PTD) [18]; protons were produced during an interval of ~150 ps. The protons were detected by a CR-39 track detector configured for imaging [15]. This approach has distinct advantages over radiography with broadband proton sources (such as intense-laser-induced sources); it allows us to optimize a special detector design and to make precise connections between particle deflections and field magnitudes.

Our experimental setup is illustrated schematically in Fig. 2. In each experiment, 14.7 MeV backlighter protons were passed through meshes with 150 μm periods (to form discrete, 75 μm beamlets with ~2000 protons each) and used to simultaneously image two separate laser-plasma interactions; one was imaged face on, while the other was imaged from the side. The laser-plasma interactions on each plastic (CH) foil were induced by a single laser *interaction* beam with wavelength 0.351 μm, incident 23° from the normal direction. The laser had a square pulse either 1 ns or 0.6 ns long, with an energy of 500 J or 250 J. The diameter of the laser beam on the foil

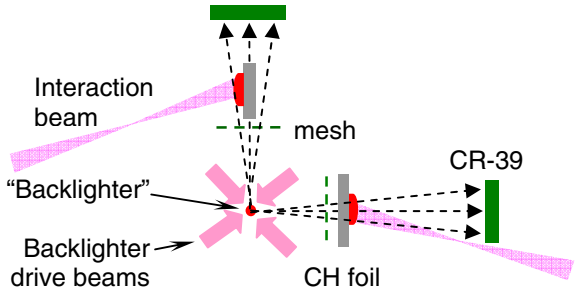

FIG. 2 (color online). Schematic illustration of our experiment setup and the physical relationship between the proton backlighter (imploded D^3He-filled capsule), mesh, CH foils, CR-39 imaging detectors, and OMEGA laser beams. The distances of components from backlighter were 0.8 cm for mesh, 1 cm for foil, and, 36 cm for detector.

(containing 95% of the energy deposition) was determined by the phase plate [19], which was either SG2 (500 μm) or SG4 (800 μm); the resulting laser intensity was of order 10^{14} W/cm^2. X-ray emissions indicate that the plasmas had $n_e \sim 10^{20}$–10^{22}/cm^3 and $T_e \sim 1$ keV.

The interaction of the laser with the CH foil was modeled with the 2D LASNEX hydrocode [20]. The B field package [21] in LASNEX includes the full Braginskii cross-field transport model and spontaneously generates fields in the presence of nonparallel T_e and n_e gradients. Proton transport through these fields and plasmas was modeled with the LSP hybrid PIC code [22]. Because only a single energy (14.7 MeV) was used, directly comparing simulations and experimental data provides unambiguous quantitative information about fields. Simulations [8] indicate that face-on radiography is largely sensitive only to the B field [23], while side-on radiography is primarily sensitive only to the E field. This allows E and B fields to be measured separately.

Figure 3(a) shows face-on images acquired from three different shots. Laser timing was adjusted so the D^3He protons arrived at the foil at 0.0, 0.33, and 0.64 ns, respectively, after the laser interaction beam was turned on. The laser beam had an SG4 phase plate, with a 1 ns, 500 J pulse. The measured images are very similar to the LASNEX + LSP simulations shown in Fig. 3(b), both in terms of the time dependence of the apparent diameter of the plasma bubble and in terms of the amount of distortion of the mesh pattern inside the plasma bubble region. Significant distortions occurred near the border of the bubble, where the proton beamlets were deflected by a strong B field and piled up to form a sharp circular ring; smaller distortion at the center indicates a smaller, but measurable B field there. These features are largely reproduced by simulations illustrated in Fig. 4, showing that toroidal B fields were concentrated

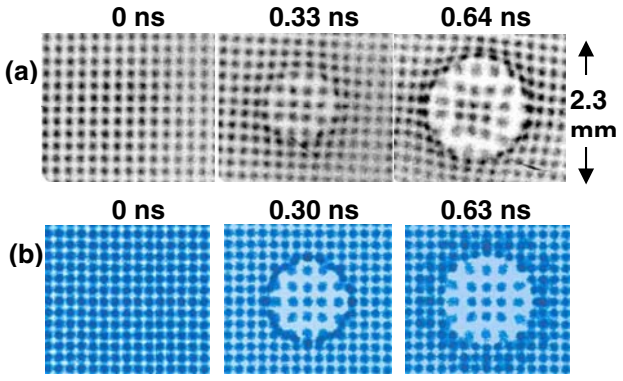

FIG. 3 (color online). (a) Measured face on, D^3He proton images showing the effects of the B field generated by laser-plasma interactions at 0.0, 0.33, and 0.64 ns, respectively, after the interaction beam was turned on. The labeled dimensions of the image are scaled to the location of the foil. (b) Images simulated by LASNEX + LSP for the conditions that produced the experimental images shown in (a).

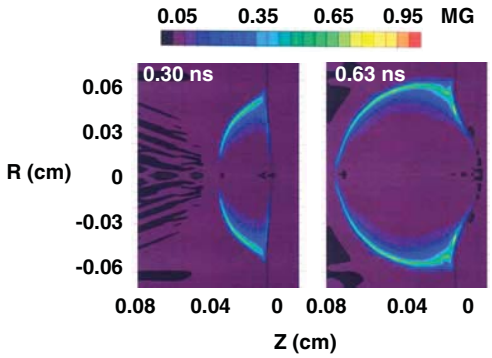

FIG. 4 (color). Time evolution of B field strength on a cross section of the plasma bubble, simulated by LASNEX for the experimental conditions of Fig. 3. In each case, the horizontal coordinate z is distance from the foil (assuming the laser is incident from the left) and the vertical coordinate R is distance from the central axis of the plasma bubble.

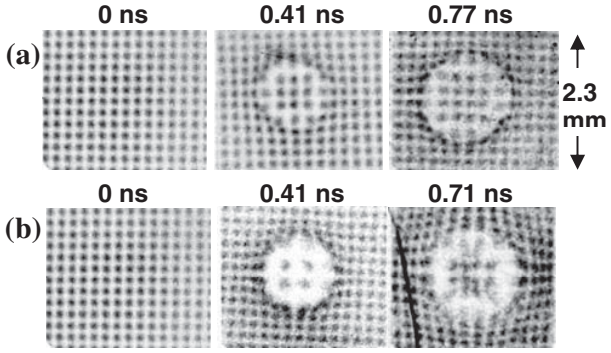

FIG. 5. D^3He-proton radiographs recorded for experiments with similar interaction laser pulse but different phase plates: (a) SG4 and (b) SG2.

on a hemispherical shell surrounding the ablative plasma bubble; they had maximum amplitude near the edge but fell to zero at the center. The B fields can be estimated from the data by using the linear displacement ξ of the beamlets in an image from where they would be without the distortion, together with the geometry of the imaging system and the scale length ($L_B \equiv B/\nabla B$) in the direction perpendicular to the image ($B \propto \xi E_p{}^{0.5} L_B{}^{-1}$). L_B was estimated to be $L_B \sim L_\parallel \equiv n_e/\nabla n_e$, which is about the radius of the bubble. This estimated L_B is within a factor of 2 of what one would infer from the simulations near the edge of the bubble. The inferred peak B values of about 0.5 MG agree well with simulations. In contrast to previous experiments and simulations, where the plasmas were usually generated by a short-pulse laser ($\sim$ 1 to 100 ps), we used long pulses which result in time evolution on a scale longer than our 150 ps sampling time; this allows us to clearly measure the time evolution of the field structure as shown in Fig. 3.

Displacements ξ of individual beamlet positions in the images represent not lateral displacements at the foil but angular deflections that result in lateral displacement at the detector. Deflection angles can be inferred directly from displacements ξ by using the experiment dimensions, but quantitative comparisons between measured and simulated images are most easily made in terms of image dimensions and values of ξ. In Fig. 3, for example, we can look at the apparent diameter of the plasma bubbles (where beamlet ''pileup'' occurs). At $\sim$0.3 ns it is about 1.5 mm for both simulation and data, though the value for the real image is harder to measure exactly because the pileup position is not as well defined. At $\sim$0.6 ns, both data and simulation show diameters of about 1.6 mm. Next we can look at the displacements ξ in the centers of the images, which are proportional to the B field in the centers of the bubbles. At $\sim$0.3 ns ξ is about 40 μm for both data and simulation, showing good agreement at that time. At 0.64 ns the agreement is not so good, since ξ is about 50 μm for the simulation but $\sim$0 for the data. Finally, we look outside the bubbles and see that the data show a slight mesh distortion that is not apparent in the simulations; the simulations may have underestimated the plasma resistivity, or the interaction laser may have had more energy in its wings than assumed in the simulations. The simulations have done a good job of modeling the overall behavior of the plasma bubble, indicating that basic physics issues were properly addressed, but there are some differences that merit further investigation.

Images acquired with different phase plates are contrasted in Fig. 5: SG4 (800 μm) and SG2 (500 μm). In all cases the laser pulses had similar energy and pulse shape ($\sim$ 250 J, 0.6 ns square), so the laser intensity for the second row was $\sim$2.6 times higher. This resulted in deflection of the central beamlets by nearly a factor of 10 more in the central region for SG2 than for SG4 at $\sim$0.4 ns, but not at $\sim$0.7 ns. This is consistent with our LASNEX simulations, which show that significant B field is generated in the central region at earlier times, but that it moves to the edge of the plasma due to the plasma expansion.

The images shown in Fig. 6 show a consequence of using no phase plate for the interaction beam. Both images were recorded around 0.3 ns and utilized similar interaction beam diameters, pulse shapes, and laser energy. Compared to the image recorded with phase plate (a), that recorded without (b) shows a more chaotic pattern, implying a B

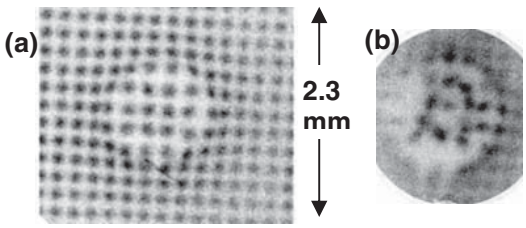

FIG. 6. Effects of phase plates on B-field structure is demonstrated by D^3He proton radiographs made using interaction beams with (a) and without (b) phase plates under conditions otherwise similar. Chaotic structure is clearly seen in image (b).

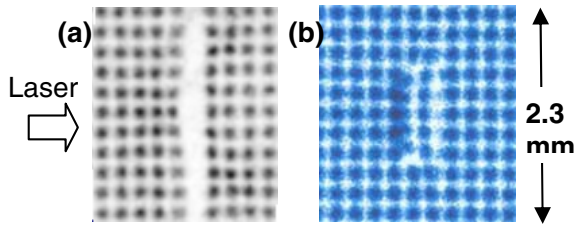

FIG. 7 (color online). Data (a) and simulation (b) for the side-on images. The distortion in the center column of (a) resulted from the E field. The large separation between the two center columns of beamlets in (a) is due to attenuation by the CH foil, which is 50 μm thick but 3 mm long in the direction parallel to the proton trajectories; this effect is not seen in (b) because proton-foil interactions were not modeled in the LSP simulation.

field with medium-scale structure (at ~20%–30% of the bubble size). This observation is consistent with theoretical expectations. An unconditioned OMEGA laser beam has nonuniformities at scales of ~40 μm. These can lead to medium-scale, random plasma structures, in particular those associated with very localized regions of strong $\nabla n_e \times \nabla T_e$, including the resonance absorptions at local oblique incidence, filaments, laser hot spots, and instabilities [1–5]. When phase plates are used, they convert the medium-scale laser nonuniformities to a smaller scale of ~2 μm (the speckle size). Short wavelength plasma structures are more easily smoothed by thermal transport than medium wavelength structures, so plasmas are more uniform when phase plates are deployed.

Side-on measured (a) and simulated (b) images are shown in Fig. 7 for the same shot that generated the center image shown in Fig. 5(b). The displacements of the beamlets away from the foil represent the effect of the E field generated by $\nabla P/n_e$. The size of the apparent beamlet displacement ($\xi \approx 60$ μm) is used to estimate the E field strength ($E \propto \xi E_p L_\perp{}^{-1}$); by assuming that the field operates over a scale length $L_\perp$ comparable to the radius of the plasma bubble, $E \approx 1.5 \times 10^8$ V/m was deduced. The magnitude of the beamlet displacement in the experiment is very similar to what is seen in the simulation.

In summary, high-resolution, time-gated proton radiography images of a plastic foil driven by a 10^{14} W/cm^2 laser were obtained and imply $|B| \sim 0.5$ MG and $|E| \sim 1.5 \times 10^8$ V/m. The experiments also demonstrated that phase plates substantially reduce medium-scale chaotic field structure. Overall, there was good agreement between experiment and LASNEX/LSP simulations, as demonstrated here for the first time, although there exist intriguing differences that merit further investigation. Experiments to be conducted soon will investigate late times in the evolution of the field structure (to long after the interaction laser has been turned off), investigate the interactions of 2 or more laser-plasma induced magnetic bubbles, and probe structures for which the 2D symmetry implicit in the LASNEX/LSP simulations will be broken.

The work described here was performed in part at the LLE National Laser User's Facility (NLUF), and was supported in part by US DOE (Grant No. DE-FG03-03SF22691), LLNL (subcontract Grant No. B504974), and LLE (subcontract Grant No. 412160-001G).

[1] S. Eliezer, *The Interaction of High-Power Lasers with Plasmas* (IOP Publishing, Bristol, 2002).
[2] L. Spitzer, *Physics of Fully Ionized Gases* (Interscience, New York, 1962).
[3] S. I. Braginskii, *Review of Plasma Physics 1* (Consultants Bureau, New York, 1965).
[4] J. A. Stamper *et al.*, Phys. Rev. Lett. **26**, 1012 (1971).
[5] M. G. Haines, Phys. Rev. Lett. **78**, 254 (1997).
[6] S. H. Glenzer *et al.*, Phys. Rev. Lett. **87**, 045002 (2001).
[7] P. A. Amendt *et al.*, Bull. Am. Phys. Soc. **49**, 26 (2004).
[8] R. P. J. Town *et al.*, Bull. Am. Phys. Soc. **50**, 123 (2005).
[9] M. A. Yates *et al.*, Phys. Rev. Lett. **49**, 1702 (1982).
[10] M. Borghesi *et al.*, Phys. Rev. Lett. **81**, 112 (1998).
[11] U. Wagner *et al.*, Phys. Rev. E **70**, 026401 (2004).
[12] A. J. Mackinnon *et al.*, Rev. Sci. Instrum. **75**, 3531 (2004).
[13] L. Romagnani *et al.*, Phys. Rev. Lett. **95**, 195001 (2005).
[14] C. K. Li *et al.*, Rev. Sci. Instrum. (to be published).
[15] F. H. Séguin *et al.*, Rev. Sci. Instrum. **74**, 975 (2003).
[16] C. K. Li *et al.*, Phys. Plasmas **7**, 2578 (2000).
[17] F. H. Séguin *et al.*, Rev. Sci. Instrum. **75**, 3520 (2004).
[18] J. A. Frenje *et al.*, Phys. Plasmas **11**, 2798 (2004).
[19] Y. Lin *et al.*, Opt. Lett. **20**, 764 (1995).
[20] G. B. Zimmerman and W. L. Kruer, Comments Plasma Phys. Control. Fusion **2**, 51 (1975).
[21] P. D. Nielsen and G. B. Zimmerman, Lawrence Livermore National Laboratory Report No. UCRL-53123, 1981.
[22] D. R. Welch *et al.*, Nucl. Instrum. Methods Phys. Res., Sect. A **464**, 134 (2001).
[23] In addition, E fields can be eliminated as a cause of deflections in face-on images by utilizing, in part, the monoenergetic character of the protons to show that on the time scale of ps electrons would short out the E fields that would be required to create the circular patterns.